IEEE Photonics Journal
An IEEE Photonics Society Publication

Propagation Properties of Gaussian Schell-Model Beam Array in the Jet Engine Exhaust Induced Turbulence

Volume 12, Number 6, December 2020

Yuqiu Zhang
Tianyue Hou
Qi Chang
Hongxiang Chang
Jinhu Long
Pengfei Ma
Pu Zhou

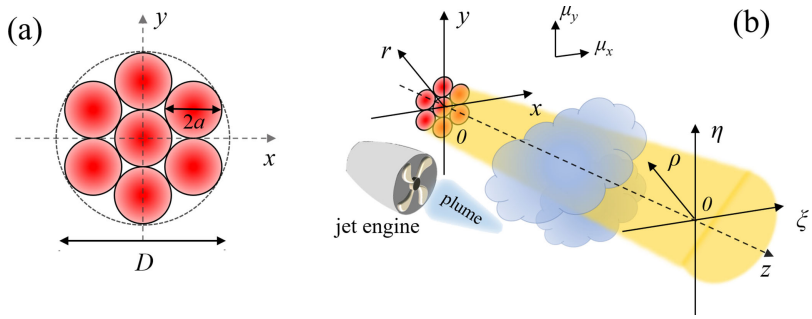

DOI: 10.1109/JPHOT.2020.3037653

Propagation Properties of Gaussian Schell-Model Beam Array in the Jet Engine Exhaust Induced Turbulence

Yuqiu Zhang, Tianyue Hou, Qi Chang, Hongxiang Chang, Jinhu Long, Pengfei Ma, and Pu Zhou

College of Advanced Interdisciplinary Studies, National University of Defense Technology, Changsha 410073, China

DOI:10.1109/JPHOT.2020.3037653

Manuscript received October 5, 2020; revised October 30, 2020; accepted November 9, 2020. Date of publication November 16, 2020; date of current version December 9, 2020. This work was supported in part by the Hunan Provincial Innovation Construct Project under Grant 2019RS3017, and in part by the Natural Science Foundation of Hunan province, China under Grant 2019JJ10005. Corresponding author: Pu Zhou (e-mail: zhoupu203@163.com).

Abstract: The effects of the jet engine turbulence on a Gaussian Schell-Model (GSM) beam array propagating in a jet engine plume are studied theoretically. The analytical expressions of the cross-spectral density (CSD) function, the spectral degree of coherence (DOC) and the mean-squared beam width for a GSM beam array propagating through a jet engine plume region are derived based on the extended Huyens-Fresnel integral. It is found that the profile of spectral density and the DOC of a GSM beam array gradually transfer to an elliptical shape as the propagation distance increases, and the elliptical degree becomes greater with increasing source coherence length. Besides, as the source coherence length decreases, the effect of the jet engine turbulence on the beam broadening is smaller and the profile of the DOC appears sidelobes at short distance. It is also found that the values of effective coherence width nearly remain the same for different values of source coherence length after propagating a certain distance. Furthermore, the effects of the number of beamlets on the beam width and effective coherence width are investigated in detail.

Index Terms: Gaussian Schell-model beam, degree of coherence, jet engine turbulence, atmospheric propagation.

1. Introduction

Until now, laser beam propagation through atmospheric turbulence has been investigated theoretically and practically for many practical applications, such as remote sensing, LIDARs, imaging systems and free space optical communication systems [1], [2]. Usually, the turbulence effect is caused by hot exhaust mixing air from the jet engine with surrounding air in the engine exhaust plume region, which can cause air refractive index fluctuations in spatial and temporal dimensions [3]. And then, these fluctuations cause laser beam wandering, broadening and intensity fluctuations while airborne laser beams propagate in the engine exhaust plume region. To describe the turbulence effects caused by a jet engine exhaust more deeply, many works have been carried out theoretically and experimentally [4]–[6]. The anisotropic power spectrum in jet engine exhaust is proposed by Sirazetdinov *et al*. [7]. In general, the typical values of structure constant C_n^2 in the jet engine exhaust induced turbulence are taken as $1 - 10 \times 10^{10}\mathrm{m}^{-2/3}$, which are several orders in magnitude larger compared with the normal atmosphere structure constant. Thus, the engine

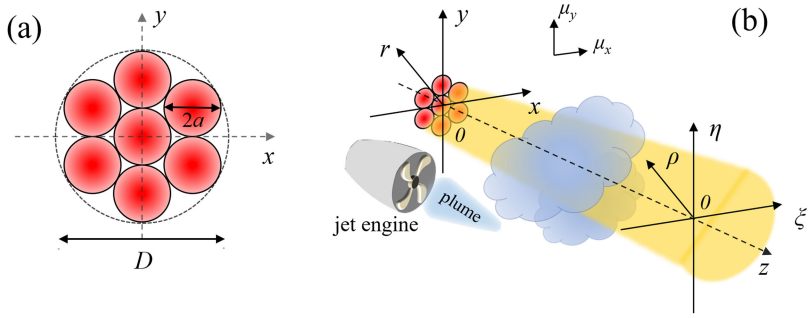

Fig. 1 Schematic diagrams of (a) a GSM beam array, and (b) beam propagation through a jet engine exhaust induced turbulence.

exhaust plumes can cause the beam quality degraded seriously. In recent years, many studies on laser beam laser beam propagating through jet engine turbulence have been reported [3]–[5], [7]–[9]. Among these studies, most reports are about fully coherence light. Recently, Ding *et al.* extended the research and investigated the propagation of GSM in jet engine turbulence [8].

On the other hand, laser array beams have widely applications in high power systems and inertial confinement fusion because of their excellent characteristics such as efficiency, compactness and reliability in high power systems [10]–[12]. Thus, it is important and necessary to investigate the propagation properties of array beam under the atmospheric and oceanic turbulence. Up to now, many works have been carried out on the propagation properties of laser array beams propagating through atmospheric and oceanic turbulence [13]–[26]. Besides, it has been found that laser beams with low coherence can suffer from smaller intensity fluctuations under influence of atmospheric turbulence [27], [28], which can improve the performance of communication systems. Therefore, the partially coherent beams have been studied detailly both in theoretically and experimentally [29]–[38]. Furthermore, With the development of the array beam in space optical communication applications, the array beam systems are gradually used on the airborne platform. Recently, Whiteley *et al.* investigated the effect of aero-optical disturbances on a conformal phased beam array located on the high-speed aircraft [39]. To the best of our knowledge, the effects of the jet engine turbulence on a GSM beam array have not been reported yet.

In this paper, considering a GSM beam array propagating through the jet engine plume region, we derive the analytical expressions of the CSD function and mean-squared beam width for a GSM beam array propagating through the jet engine plume region based on the extended Huyens-Fresnel integral. Moreover, we investigate the beam width, the spectral degree of spatial coherence and the number of beamlets of a GSM beam array propagating in a jet engine plume on propagation properties by numerical simulation.

2. Propagation of a GSM Beam Array in the Jet Engine Plume Region

Consider a GSM beam array is composed of numbers of N GSM beamlets located at the source plane ($z = 0$), as shown in Fig. 1(a). The diameters of beamlet and effective exit aperture are $2a$ and D, respectively. Consider the GSM beamlets are correlated and perfect replicas of each other. The cross-spectral density (CSD) function of GSM beam array at the $z = 0$ plane can be expressed as [40]

$$W^{(0)}(\boldsymbol{r}_1, \boldsymbol{r}_2, \omega) = \sum_{m=1}^{N}\sum_{n=1}^{N} \exp\left[-\frac{(\boldsymbol{r}_1 - \boldsymbol{r}_m)^2 + (\boldsymbol{r}_2 - \boldsymbol{r}_n)^2}{w_0^2}\right] \exp\left\{-\frac{[(\boldsymbol{r}_2 - \boldsymbol{r}_n) - (\boldsymbol{r}_1 - \boldsymbol{r}_m)]^2}{2\delta_0^2}\right\}, \quad (1)$$

where $\boldsymbol{r}_1 = (x_1, y_1)$ and $\boldsymbol{r}_2 = (x_2, y_2)$ are the two-dimensional position vectors perpendicular to the direction of the beam propagation in the transverse plane, $\boldsymbol{r}_m = (x_m, y_m)$ and $\boldsymbol{r}_n = (x_n, y_n)$ are the center of the mth and nth beamlets, w_0 and δ_0 denote the waist width and spatial correlation length

of the beamlets, respectively, and ω is the angular frequency. It is noted that we assume the GSM beam array is quasi-monochromatic. For brevity, the dependence of the CSD function on ω is omitted in this paper.

Let a GSM beam array source located in the $z = 0$ plane propagating along direction z in a jet engine exhaust induced turbulence (see Fig. 1(b)). By using the extended Huygens-Fresnel principle and paraxial approximation, the CSD function of the GSM beam array after propagation through a jet engine exhaust induced turbulence is defined as [41]

$$W(\boldsymbol{\rho}_1, \boldsymbol{\rho}_2, z) = \frac{k^2}{(2\pi z)^2} \int_{-\infty}^{\infty} \int_{-\infty}^{\infty} W^{(0)}(\boldsymbol{r}_1, \boldsymbol{r}_2) exp\left\{\frac{ik}{2z}\left[-(\boldsymbol{\rho}_1 - \boldsymbol{r}_1)^2 + (\boldsymbol{\rho}_2 - \boldsymbol{r}_2)^2\right]\right\} \times \left\langle \exp\left[\psi^*(\boldsymbol{r}_1, \boldsymbol{\rho}_1, z) + \psi(\boldsymbol{r}_2, \boldsymbol{\rho}_2, z)\right]\right\rangle d^2\boldsymbol{r}_1 d^2\boldsymbol{r}_2, \tag{2}$$

where $\boldsymbol{\rho}_1 = (\xi_1, \eta_1)$ and $\boldsymbol{\rho}_2 = (\xi_2, \eta_2)$ denote the two-dimensional position vectors at the receiver plane ($z > 0$), k is the wave number related to the wave length $k = 2\pi/\lambda$. For general anisotropic power spectra of turbulence, the last term in the integrand of Eq. (2) can be expressed as [42]

$$\left\langle \exp\left[\psi * (\boldsymbol{r}_1, \boldsymbol{\rho}_1, z) + \psi(\boldsymbol{r}_2, \boldsymbol{\rho}_2, z)\right]\right\rangle = \exp\left\{-4\pi^2 k^2 z \int_0^1 dt \int_0^{\infty} \kappa d\kappa \Phi_n(\kappa)\left[1 - J_0\left(\left|t(\boldsymbol{\rho}_1 - \boldsymbol{\rho}_2) + (1-t)(\boldsymbol{r}_1 - \boldsymbol{r}_2)\right| \cdot \kappa\right)\right]\right\}, \tag{3}$$

where $J_0(\cdot)$ is the Bessel function of the first kind and zero order. κ is the magnitude of two-dimensional spatial frequency. Considering propagation of laser beam within a jet engine exhaust induced turbulence region, the anisotropic power spectrum proposed by Sirazetdinov *et al*. [7], [8]

$$\Phi_n(\kappa) = \Phi_{n1}(\kappa) + \Phi_{n2}(\kappa) \tag{4}$$

with

$$\Phi_{n1}(\kappa) = 0.033 C_n^2 \cdot \frac{(L_{0x}L_{0y})^{11/6}}{\left[1 + (\kappa_x L_{0x})^2 + (\kappa_y L_{0y})^2\right]^{11/6}} \exp\left(-\frac{\kappa_x^2}{\kappa_{mx}^2} - \frac{\kappa_y^2}{\kappa_{my}^2}\right), \tag{5}$$

$$\Phi_{n2}(\kappa) = 0.033 C_n^2 \cdot Q\left[\left(\frac{2\pi}{L_s}\right)^2 + \kappa^2\right]^{-\frac{11}{6}} \exp\left(-\kappa^2/\kappa_m^2\right). \tag{6}$$

Where $\kappa = \sqrt{\kappa_x^2 + \kappa_y^2}$, C_n^2 is the generalized index of refraction structure constant denoting the strength of turbulence; L_{0x} and L_{0y} are anisotropic outer scale length in the x and y directions, respectively; $\kappa_m = c(\alpha)/l_0$ with $l_0 = \sqrt{l_{0x}^2 + l_{0y}^2}$ being the inner scale, $\kappa_{mx} = c(\alpha)/l_{0x}$, $\kappa_{my} = c(\alpha)/l_{0y}$ with l_{0x} and l_{0y} being the inner scale in the x and y directions, respectively. The parameters Q and L_s are obtained by fitting to experimental data. Ding *et al*. has shown that the inner scale has a noticeable impact when the power spectrum is in the high spatial frequency region [8]. Further, the parameter $c(\alpha)$ is defined as

$$c(\alpha) = \left[\frac{2\pi\Gamma(5 - \alpha/2)A(\alpha)}{3}\right]^{\frac{1}{\alpha-5}}, \tag{7}$$

where

$$A(\alpha) = \frac{1}{4\pi^2}\Gamma(\alpha - 1)\cos\left(\frac{\alpha\pi}{2}\right), 3 < \alpha < 4. \tag{8}$$

Here, $\Gamma(.)$ is the Gamma function, and α is the power-law exponent. According to Eqs. (4)–(6), Eq. (3) can be rewritten as follows

$$\left\langle \exp\left[\psi * (\boldsymbol{r}_1, \boldsymbol{\rho}_1, z) + \psi(\boldsymbol{r}_2, \boldsymbol{\rho}_2, z)\right]\right\rangle = A + B, \tag{9}$$

where

$$A = \exp\left\{-4\pi^2 k^2 z \int_0^1 \mathrm{d}t \int_0^\infty \kappa \mathrm{d}\kappa\, \Phi_{n1}(\kappa)\left[1 - J_0\left(\left|t\left(\boldsymbol{\rho}_1 - \boldsymbol{\rho}_2\right) + (1-t)\left(\boldsymbol{r}_1 - \boldsymbol{r}_2\right)\right| \cdot \kappa\right)\right]\right\}, \tag{10}$$

$$B = \exp\left\{-4\pi^2 k^2 z \int_0^1 \mathrm{d}t \int_0^\infty \kappa \mathrm{d}\kappa\, \Phi_{n2}(\kappa)\left[1 - J_0\left(\left|t\left(\boldsymbol{\rho}_1 - \boldsymbol{\rho}_2\right) + (1-t)\left(\boldsymbol{r}_1 - \boldsymbol{r}_2\right)\right| \cdot \kappa\right)\right]\right\}. \tag{11}$$

Now, we will calculate Eqs. (10) and (11) respectively. For term A, by using the coordinates changes $\kappa_x = \kappa_x'/\mu_x$, $\kappa_y = \kappa_y'/\mu_y$ (μ_x and μ_y denote the anisotropic factors in two mutually directions), it can be expressed as

$$A = \exp\left\{-\frac{4\pi^2 k^2 z}{\mu_x \mu_y} \int_0^1 \mathrm{d}t \int_0^\infty \int_0^\infty \mathrm{d}\kappa_x' \mathrm{d}\kappa_y' \Phi_{n1}'(\kappa')\left[1 - J_0\left(\left|t\left(\boldsymbol{\rho}_1{}' - \boldsymbol{\rho}_2{}'\right) + (1-t)\left(\boldsymbol{r}_1{}' - \boldsymbol{r}_2{}'\right)\right| \cdot \kappa'\right)\right]\right\}, \tag{12}$$

where

$$\Phi_{n1}'\left(\kappa'\right) = 0.033 C_n^2 \cdot \left(\frac{\mu_x \mu_y L_0^2}{1 + \kappa'^2 L_0^2}\right)^{\frac{11}{6}} \exp\left(-\frac{l_0^2}{c(\alpha)^2}\kappa'^2\right). \tag{13}$$

Here, $\boldsymbol{r}_j{}' = (x_j/\mu_x, y_j/\mu_y)$ and $\boldsymbol{\rho}_j{}' = (\xi_j/\mu_x, \eta_j/\mu_y)$ ($j = x$ and y). It is noted that the outer and inner scales in the x and y directions can be expressed as $L_x = \mu_x L_0$, $L_y = \mu_y L_0$, $l_x = \mu_x l_0$ and $l_y = \mu_y l_0$ with considering the ratio of the outer and inner scales in the x and y directions are constant, i.e., μ_x/μ_y.

Under the paraxial approximation, the Bessel function in Eq. (12) can be expressed as $J_0(x) \approx 1 - x^2/4$. Here, we convert Cartesian coordinate to polar coordinate, i.e., $\mathrm{d}\kappa_x'\mathrm{d}\kappa_y' = \kappa'\mathrm{d}\kappa'\mathrm{d}\theta$. By applying the above approximating and after integrating over θ, t and κ', Eq. (12) becomes

$$\begin{aligned} A = & \exp\left\{-\frac{\pi^2 k^2 z T_A\left[(\xi_1 - \xi_2)^2 + (\xi_1 - \xi_2)(x_1 - x_2) + (x_1 - x_2)^2\right]}{3\mu_x^2}\right\} \\ & \times \exp\left\{-\frac{\pi^2 k^2 z T_A\left[(\eta_1 - \eta_2)^2 + (\eta_1 - \eta_2)(y_1 - y_2) + (y_1 - y_2)^2\right]}{3\mu_y^2}\right\}, \end{aligned} \tag{14}$$

where

$$\begin{aligned} T_A &= \frac{1}{\mu_x \mu_y} \int_0^\infty \kappa'^3 \Phi_{n1}'(\kappa')\mathrm{d}\kappa' \\ &= 0.033 C_n^2 \left(\mu_x \mu_y\right)^{\frac{5}{6}} \left[\frac{\left(5 + \frac{6}{\kappa_m^2 L_0^2}\right)\exp\left(\frac{1}{\kappa_m^2 L_0^2}\right)\Gamma\left(\frac{1}{6}, \frac{1}{\kappa_m^2 L_0^2}\right)}{10\left(\frac{1}{\kappa_m^2}\right)^{\frac{1}{6}}} - \frac{3}{5}\left(\frac{1}{L_0^2}\right)^{\frac{1}{6}}\right]. \end{aligned} \tag{15}$$

Here, Γ (.,.) is the incomplete Gamma function. On substituting from Eq. (14) into Eq. (2) and by applying sum and difference vector notation $\boldsymbol{u} = (\boldsymbol{\rho}_1 + \boldsymbol{\rho}_2)/2$, $\boldsymbol{v} = \boldsymbol{\rho}_1 - \boldsymbol{\rho}_2$, the CSD function of the GSM beam array from term A can be expressed as a product

$$W_A(\boldsymbol{\rho}_1, \boldsymbol{\rho}_2, z) = W_{xA}(\xi_1, \xi_2) W_{yA}(\eta_1, \eta_2), \tag{16}$$

with

$$W_{xA}\left(\xi_1, \xi_2, z\right) = \frac{1}{\sqrt{\Delta_{xA}}} \sum_{m=1}^{N} \sum_{n=1}^{N} \exp\left[\left(-\frac{1}{w_0^2 \Delta_{xA}}\right)\left(\xi_1^2 + \xi_2^2\right)\right] \exp\left[\left(-\frac{ik}{2R_{xA}}\right)\left(\xi_1^2 - \xi_2^2\right)\right]$$

$$\times \exp\left[\left(-\frac{1}{2\delta_0^2\Delta_{xA}}-\frac{\pi^2k^2zT_A}{3\mu_x^2}\left(1+\frac{2}{\Delta_{xA}}\right)+\frac{2\pi^4k^2z^4T_A^2}{9w_0^2\mu_x^4\Delta_{xA}}\right)(\xi_1-\xi_2)^2\right]$$
$$\times \exp\left[C_{xA}(\xi_1-\xi_2)+D_{xA}(\xi_1+\xi_2)+E_{xA}\right]. \tag{17}$$

Where the parameters in Eq. (17) are given by

$$\Delta_{xA}=1+\left(\frac{4}{k^2w_0^4}+\frac{4}{k^2w_0^2\delta_0^2}+\frac{8\pi^2k^2zT_A}{3k^2w_0^2\mu_x^2}\right)z^2, \tag{18}$$

$$R_{xA}=z+\frac{w_0^2z/4-\pi^2T_Az^4/3\mu_x^2}{(\Delta_{xA}-1)\,w_0^2/4+\pi^2T_Az^3/3\mu_x^2}, \tag{19}$$

$$C_{xA}=\left(-\frac{w_0^2k^2}{4z^2\Delta_{xA}}+\frac{w_0^2k^2}{4z^2}-\frac{\pi^2k^2T_Az}{3\mu_x^2\Delta_{xA}}+\frac{8\pi^4k^2z^4T_A^2}{9w_0^2\mu_x^4\Delta_{xA}}-\frac{\pi^2k^2T_Az}{3\mu_x^2}\right)(x_m-x_n)$$
$$+\left(-\frac{ik}{2z\Delta_{xA}}+\frac{ik}{2z}+\frac{2i\pi^2kT_Az^2}{3\mu_x^2w_0^2\Delta_{xA}}\right)(x_m+x_n), \tag{20}$$

$$D_{xA}=\left(-\frac{ik}{2z\Delta_{xA}}+\frac{ik}{2z}-\frac{4i\pi^2kT_Az^2}{3\mu_x^2w_0^2\Delta_{xA}}\right)(x_m-x_n)+\left(\frac{1}{w_0^2\Delta_{xA}}\right)(x_m+x_n), \tag{21}$$

$$E_{xA}=\left[\left(\frac{w_0^2k^2}{8z^2\Delta_{xA}}-\frac{w_0^2k^2}{8z^2}+\frac{8\pi^4k^2z^4T_A^2}{9\mu_x^4w_0^2\Delta_{xA}}+\frac{2\pi^2k^2T_Az}{3\mu_x^2\Delta_{xA}}-\frac{\pi^2k^2zT_A}{3\mu_x^2}\right)(x_m-x_n)^2\right]$$
$$\times\left[-\frac{1}{2w_0^2\Delta_{xA}}(x_m+x_n)^2+\left(\frac{ik}{2z\Delta_{xA}}-\frac{ik}{2z}+\frac{4i\pi^2kT_Az^2}{3\mu_x^2w_0^2\Delta_{xA}}\right)(x_m^2-x_n^2)\right], \tag{22}$$

In the same way, we can get the expression of W_{yA} by replacing x, ξ_1 and ξ_2 with y, η_1, η_2, respectively.

For term B, by adopting the same approach as term A, the Eq. (11) can be obtained

$$B=\exp\left\{-\frac{\pi^2k^2zT_B\left[(\xi_1-\xi_2)^2+(\xi_1-\xi_2)(x_1-x_2)+(x_1-x_2)^2\right]}{3}\right\}$$
$$\times\exp\left\{-\frac{\pi^2k^2zT_B\left[(\eta_1-\eta_2)^2+(\eta_1-\eta_2)(y_1-y_2)+(y_1-y_2)^2\right]}{3}\right\}, \tag{23}$$

where

$$T_B=\int_0^\infty\kappa^3\Phi_{n2}(\kappa)\mathrm{d}\kappa=0.033C_n^2Q\left[\frac{\left(5+\frac{24\pi^2}{\kappa_m^2L_s^2}\right)\exp\left(\frac{4\pi^2}{\kappa_m^2L_s^2}\right)\Gamma\left(\frac{1}{6},\frac{4\pi^2}{\kappa_m^2L_s^2}\right)}{10\left(\frac{1}{\kappa_m^2}\right)^{\frac{1}{6}}}-\frac{3}{5}\left(\frac{4\pi^2}{L_s^2}\right)^{\frac{1}{6}}\right]. \tag{24}$$

On substituting from Eq. (23) into Eq. (2), the CSD function of the GSM beam array from term B can be expressed as a product

$$W_B(\boldsymbol{\rho}_1,\boldsymbol{\rho}_2,z)=W_{xB}(\xi_1,\xi_2)W_{yB}(\eta_1,\eta_2), \tag{25}$$

with

$$W_{xB}(\xi_1,\xi_2,z)=\frac{1}{\sqrt{\Delta_B}}\sum_{m=1}^{N}\sum_{n=1}^{N}\exp\left[\left(-\frac{1}{w_0^2\Delta_B}\right)(\xi_1^2+\xi_2^2)\right]\exp\left[\left(-\frac{ik}{2R_B}\right)(\xi_1^2-\xi_2^2)\right]$$

$$\times \exp\left[\left(-\frac{1}{2\delta_0^2\Delta_B}-\frac{\pi^2k^2zT_B}{3}\left(1+\frac{2}{\Delta_B}\right)+\frac{2\pi^4k^2z^4T_B^2}{9w_0^2\Delta_B}\right)(\xi_1-\xi_2)^2\right]$$
$$\times \exp\left[C_{xB}(\xi_1-\xi_2)+D_{xB}(\xi_1+\xi_2)+E_{xB}\right]. \tag{26}$$

Where the parameters in Eq. (26) are given by

$$\Delta_B = 1+\left(\frac{4}{k^2w_0^4}+\frac{4}{k^2w_0^2\delta_0^2}+\frac{8\pi^2k^2zT_B}{3k^2w_0^2}\right)z^2, \tag{27}$$

$$R_B = z+\frac{w_0^2z/4-\pi^2T_Bz^4/3}{(\Delta_B-1)\,w_0^2/4+\pi^2T_Bz^3/3}, \tag{28}$$

$$C_{xB} = \left(-\frac{w_0^2k^2}{4z^2\Delta_{xB}}+\frac{w_0^2k^2}{4z^2}-\frac{\pi^2k^2T_Bz}{3\Delta_{xB}}+\frac{8\pi^4k^2z^4T_B^2}{9w_0^2\Delta_{xB}}-\frac{\pi^2k^2T_Bz}{3}\right)(x_m-x_n)$$
$$+\left(-\frac{ik}{2z\Delta_{xB}}+\frac{ik}{2z}+\frac{2i\pi^2kT_Bz^2}{3w_0^2\Delta_{xB}}\right)(x_m+x_n), \tag{29}$$

$$D_{xB} = \left(-\frac{ik}{2z\Delta_{xB}}+\frac{ik}{2z}-\frac{4i\pi^2kT_Bz^2}{3w_0^2\Delta_{xB}}\right)(x_m-x_n)+\left(\frac{1}{w_0^2\Delta_{xB}}\right)(x_m+x_n), \tag{30}$$

$$E_{xB} = \left[\left(\frac{w_0^2k^2}{8z^2\Delta_{xB}}-\frac{w_0^2k^2}{8z^2}+\frac{8\pi^4k^2z^4T_B^2}{9w_0^2\Delta_{xB}}+\frac{2\pi^2k^2T_Bz}{3\Delta_{xB}}-\frac{\pi^2k^2zT_B}{3}\right)(x_m-x_n)^2\right]$$
$$\times\left[-\frac{1}{2w_0^2\Delta_{xB}}(x_m+x_n)^2+\left(\frac{ik}{2z\Delta_{xB}}-\frac{ik}{2z}+\frac{4i\pi^2kT_Bz^2}{3w_0^2\Delta_{xB}}\right)(x_m^2-x_n^2)\right], \tag{31}$$

In the same way, we can get the expression of W_{yB} by replacing x, ξ_1 and ξ_2 with y, η_1, η_2, respectively. Thus, the CSD function of GSM beam array propagation through a jet engine exhaust can be expressed as

$$W(\boldsymbol{\rho}_1,\boldsymbol{\rho}_2,z) = W_A(\boldsymbol{\rho}_1,\boldsymbol{\rho}_2,z)+W_B(\boldsymbol{\rho}_1,\boldsymbol{\rho}_2,z). \tag{32}$$

Noted that for $\boldsymbol{r}_m=\boldsymbol{r}_n=0$, Eq. (32) reduce to the CSD of a GSM beam, which is consistent with the result in Ref. [8]. On substituting $\boldsymbol{\rho}_1=\boldsymbol{\rho}_2=\boldsymbol{\rho}$ into Eq. (32), the spectral density $I(\boldsymbol{\rho},z)$ can be obtained.

The influence of the jet engine exhaust on the coherence properties can be learned by the spectral degree of spatial coherence (DOC), and the DOC signify the statistical properties between a pair of points at locations $T_1(-\boldsymbol{\rho},z)$ and $T_2(\boldsymbol{\rho},z)$ can be expressed as [41]

$$\mu(-\boldsymbol{\rho},\boldsymbol{\rho},z) = \frac{W_A(-\boldsymbol{\rho},\boldsymbol{\rho},z)+W_B(-\boldsymbol{\rho},\boldsymbol{\rho},z)}{\sqrt{[W_A(-\boldsymbol{\rho},-\boldsymbol{\rho},z)+W_B(-\boldsymbol{\rho},-\boldsymbol{\rho},z)]}\sqrt{[W_A(\boldsymbol{\rho},\boldsymbol{\rho},z)+W_B(\boldsymbol{\rho},\boldsymbol{\rho},z)]}}. \tag{33}$$

Furthermore, the effective width of the DOC (effective coherence width) is defined as the point drops from its maximum value (i.e., at $\rho=0$) to the $1/e^2$ in this paper.

3. Numerical Results and Discussions

In this section, we will investigate the propagation characteristics of a GSM beam array in the jet engine exhaust induced turbulence based on the analytical expressions derived in section 2. It is noted that the turbulence parameters we choose are based on the researches of Ref. [3]. Unless specified, the initial parameters are taken as $w_0=0.01$ m, $a=0.015$ m, $\lambda=632.8$ nm, $N=7$, $\alpha=11/3$, $C_n^2=1.6\times10^{-9}$ m$^{-2/3}$, $L_0=0.5$ m, $L_S=1$ mm, $l_0=2/3$ mm, $\mu_x=0.7$, $\mu_y=1.4$, $Q=6$.

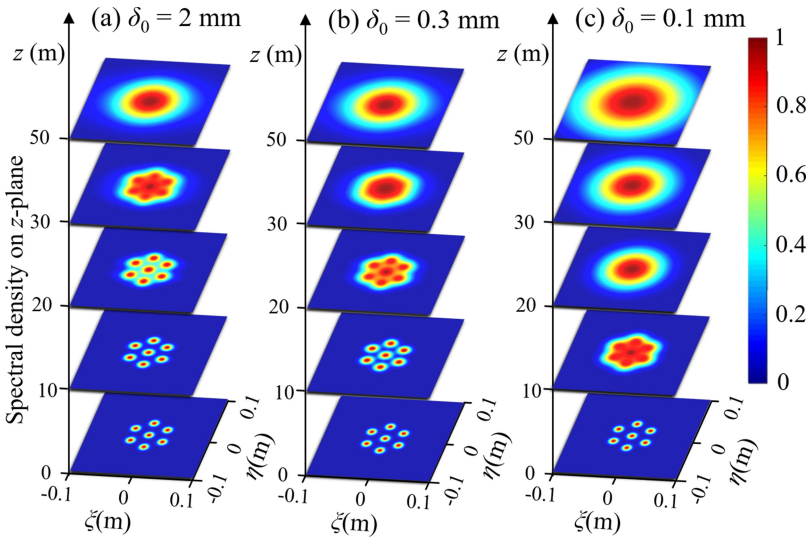

Fig. 2. Normalized spectral density patterns of GSM beam array at different propagation distances in jet engine exhaust region for different values of source coherence length δ_0.

The normalized spectral density distributions at different propagation distances for three different values of source coherence length δ_0 are shown in Fig. 2, where the normalized spectral density is normalized with respect to its own maximum value. It can be seen from Fig. 2 that a significant beam broadening of the GSM beam array emerges when the beam propagation distance is on the order of meters, due to the typical values of structure constant in the jet engine plume region are several orders in magnitude larger compared with the normal atmosphere structure constant. It can be seen from Figs. 2(a) and 2(b) that the beam shape becomes elliptical as the $\delta_0 = 2$ mm and 0.3 mm at $z = 50$ m, while the beam shape remains approximately circle as $\delta_0 = 0.1$ mm at the same propagation distance. Thus, the beam profile can keep Gaussian distribution better as the source coherence length δ_0 decreases.

3.1 The Mean-Squared Spatial Width

In this section, we further study the evolution of mean-squared spatial width to investigate more about the GSM beam array propagation properties in the jet engine plume region, and the mean-squared spatial width is defined as [43]

$$w_j^2 = \frac{4\int\int j^2 I(x, y, z)\,\mathrm{d}x\mathrm{d}y}{\int\int I(x, y, z)\mathrm{d}x\mathrm{d}y}, \tag{34}$$

where $j = x$ and y, w_x and w_y denote the mean-squared spatial width along the x and y directions respectively. On substituting Eq. (32) into Eq. (34), we can obtain the beam width for a GSM beam array

$$w_j = \sqrt{\begin{array}{l}\sum_{a=1}^{N}\sum_{b=1}^{N}\frac{1}{F_{AB}}w_0^2\Delta_{xA}\left(1+w_0^2\Delta_{xA}D_{xA}^2\right)\exp\left\{\frac{1}{2}w_0^2\left(\Delta_{xA}D_{xA}^2+\Delta_{yA}D_{yA}^2\right)+E_{xA}+E_{yA}\right\}\\ +\sum_{a=1}^{N}\sum_{b=1}^{N}\frac{1}{F_{AB}}w_0^2\Delta_{xB}\left(1+w_0^2\Delta_{xB}D_{xB}^2\right)\exp\left\{\frac{1}{2}w_0^2\left(\Delta_{xB}D_{xB}^2+\Delta_{yB}D_{yB}^2\right)+E_{xB}+E_{yB}\right\}\end{array}}. \tag{35}$$

where

$$F_{AB} = \sum_{a=1}^{N}\sum_{b=1}^{N}\exp\left\{\frac{1}{2}w_0^2\left(\Delta_{xA}D_{xA}^2+\Delta_{yA}D_{yA}^2+\Delta_{xB}D_{xB}^2+\Delta_{yB}D_{yB}^2\right)+E_{xA}+E_{yA}+E_{xB}+E_{yB}\right\}. \tag{36}$$

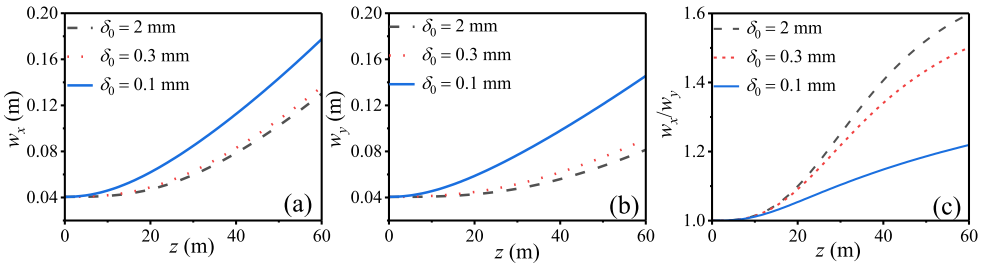

Fig. 3. For different values of source coherence length δ_0, (a) w_x, (b) w_y, and (c) w_x/w_y versus propagation distance z.

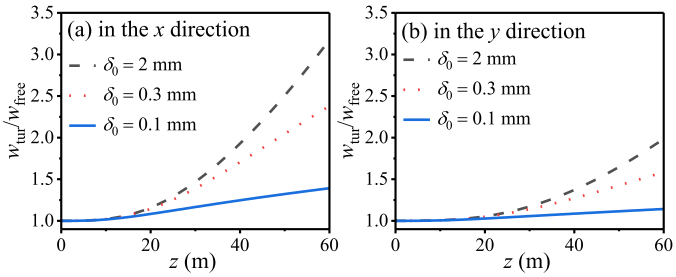

Fig. 4. The ratio of beam width in the turbulence (w_{tur}) and in free space (w_{free}).

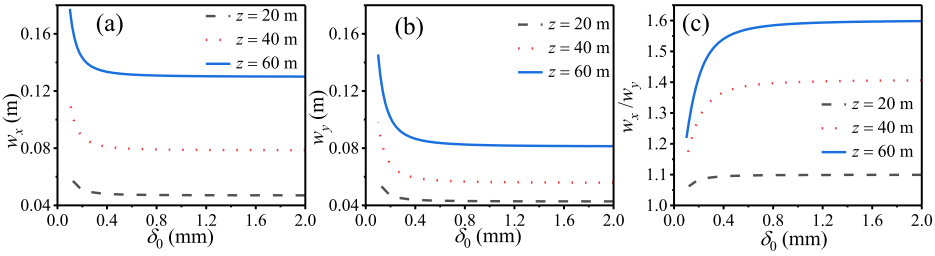

Fig. 5. For different values of propagation distance z, (a) w_x, (b) w_y, and (c) w_x/w_y versus coherence length δ_0.

According to Eqs. (35) and (36), we investigate the effect of the jet engine turbulence on the beam width of a GSM beam array propagating in the jet engine plumes. Fig. 3 shows the beam width w_{x} and w_y in the x and y directions and the ratio of w_{x} to w_y versus propagation distance z for different coherence lengths δ_0, respectively. It can be seen from Figs. 3(a) and 3(b) that the beam width increases with decreasing δ_0 at the same propagation distance. However, the different increments of beam width in the x and y directions induce the generation of elliptical beam profile shape. From Fig. 3(c), it can be seen that the value of w_{x}/w_y increases as δ_0 increases, i.e., the elliptical shape becomes more significant with increasing δ_0. To investigate the effect of the jet engine turbulence on beam broadening for different source coherence lengths, we present the ratio of beam width in jet engine turbulence (w_{tur}) and in free space (w_{free}) in Fig. 4. As can be seen that the value of $w_{\mathrm{tur}}/w_{\mathrm{free}}$ increases as z increases or δ_0 increases. It is obvious that the smaller value of $w_{\mathrm{tur}}/w_{\mathrm{free}}$ means a greater turbulence resistance. Therefore, we can know that the low coherence can weaken the effect of the jet engine turbulence, which is consistent with the results in Ref. [28].

Fig. 5 shows the beam width w_x and w_y in the x and y directions and the ratio of w_x to w_y versus coherence length δ_0 at different propagation distances z, respectively. Fig. 5 reveals that the values

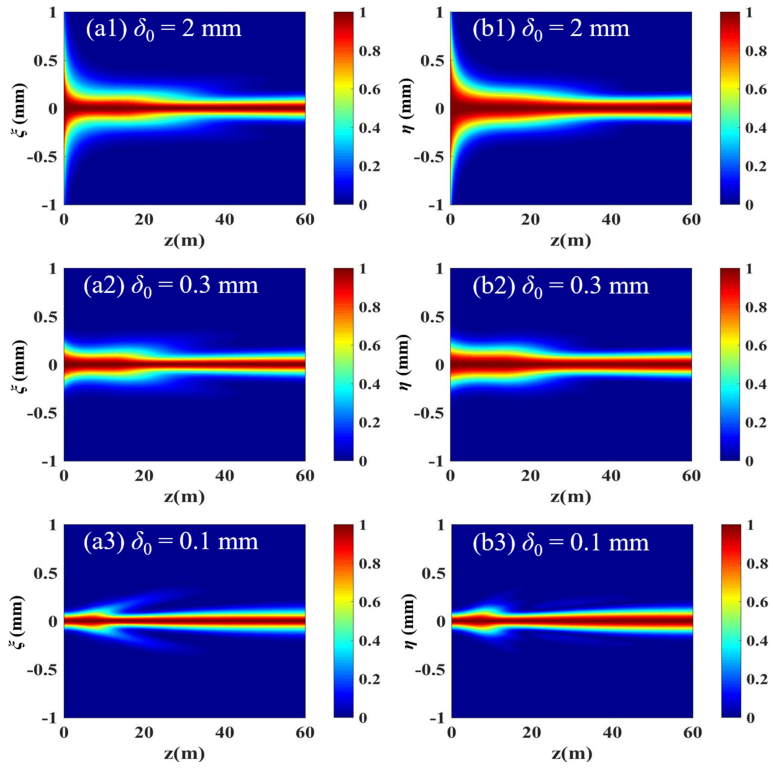

Fig. 6. The cross section of the DOC for different source coherence lengths δ_0 versus the propagation distance z in the x and y directions respectively.

of w_x and w_y decrease rapidly at first and keep almost unchanged with increasing δ_0 (see Figs. 5(a) and 5(b)). However, the value of w_x/w_y (i.e., the elliptical degree) becomes larger with increasing δ_0 (see Fig. 5(c)). In other words, small beam spot and high turbulence resistance cannot be achieved simultaneously. Thus, there should be a trade-off between small beam spot and high turbulence resistance.

3.2 The Mean-Squared Spatial Width

According to the Eq. (33), the cross section of the DOC of a GSM beam array versus propagation distance z for different source coherence lengths δ_0 through a jet engine plume is shown in Fig. 6. Figs. 6(a1)-6(a3) and Figs. 6(b1)-6(b3) show the DOC versus the propagation distance z in the x and y directions, respectively. From Fig. 6, one can see that the width of the DOC decreases with increasing propagation distance z both in the x and y directions, i.e., the spatial coherence becomes worse with increasing z due to the turbulence effect. In addition, the DOC profile is compressed more rapidly as δ_0 increases at initial propagation stage, that is to say, the effect of the jet engine turbulence on spatial coherence is more severe as δ_0 increases.

Fig. 7 shows the modulus of the DOC of a GSM beam array at different propagation distances z for different source coherence lengths δ_0. From Fig. 7(a), we can see that the DOC profile becomes elliptical at a very short distance when the δ_0 is large (see Fig. 7(a)). However, as the δ_0 decreases, the DOC profile transition to elliptical becomes less noticeable (see Figs. 7(b) and 7(c)). Meanwhile, the profile of the DOC appears sidelobes and resembles the spectral density in free space at $z =$ 10 m when the $\delta_0 =$ 0.1 mm. Comparing Figs. 6 and 7, the sidelobes of the DOC profile are more obvious and appears at a shorter distance as the δ_0 decreases. Consequently, the GSM beam array with a smaller source coherence length can weaken the effect of the jet engine turbulence and keep its own spatial coherence better.

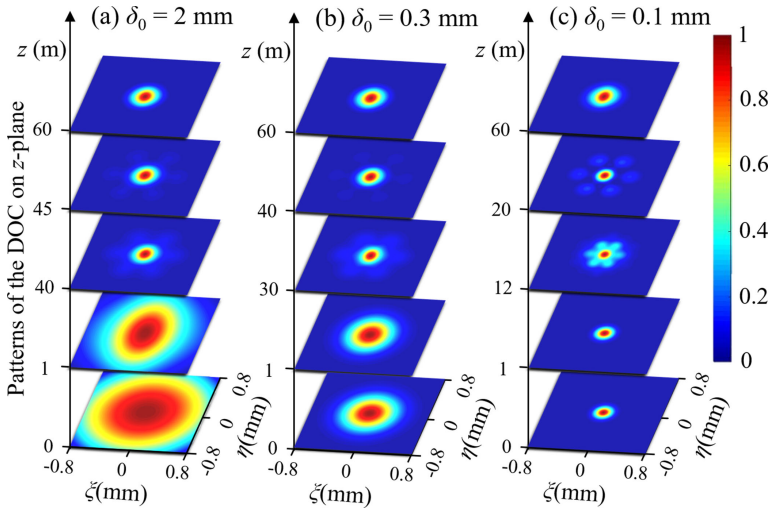

Fig. 7. The modulus of the DOC of a GSM beam array at different propagation distances for different source coherence lengths δ_0.

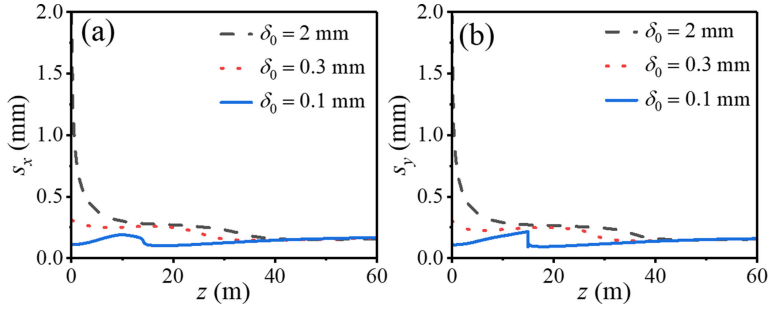

Fig. 8. The effective widths of the DOC s_x and s_y in the x and y directions, respectively.

Fig. 8 displays the effective coherence widths s_x and s_y in the x and y directions, respectively. It is obvious in Fig. 8 that the effective coherence width decreases more rapidly with increasing δ_0 at a short initial stage, and then decreases slowly in the subsequent propagation distance. However, when the $\delta_0 > 0.3$ mm, the effective width of the DOC increases at first and displays the non-monotonic changes as z increases, which is different from the situation of $\delta_0 > 0.3$ mm. The main reason is that low coherence will weaken the effect of turbulence and keep effective coherence width almost unchanged. It is noted that s_y suddenly decreases at propagation distance about 15 m because of the appearance of obvious sidelobes. In addition, we can see that the values of effective coherence width both in x and y directions nearly remain the same for different values of source coherence length after $z = 40$ m.

3.3 Number of Beamlets

In this section, we investigate the propagation properties of different number of beamlets N of the GSM beam array propagating through a jet engine exhaust. Considering the effective exit aperture D and the truncation parameter $f = w_0/a$ remain unchanged for different number of beamlets, therefore, the values of beam waist width w_0 are taken as 0.03 m, 0.01 m and 0.006 m for $N = 1$, 7 and 19, respectively. The source coherence lengths δ_0 is taken as 2 mm. In Fig. 9, we obtain the normalized spectral density distribution patterns of GSM beam array at different propagation distances in jet engine exhaust region for different number of N beamlets. From Fig. 9, we can

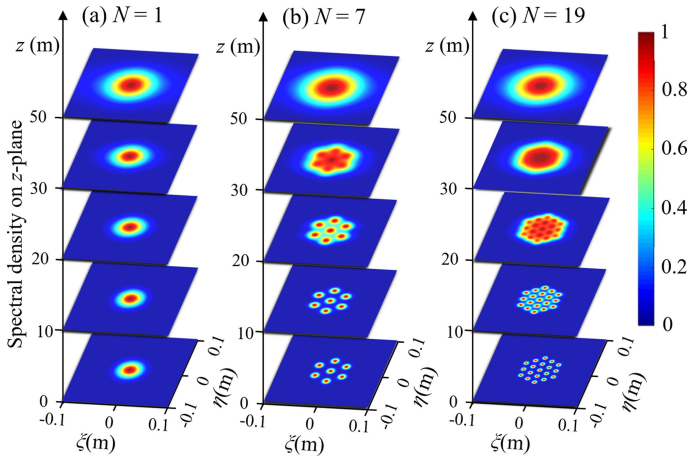

Fig. 9. Normalized spectral density patterns of GSM beam array at different propagation distances in jet engine exhaust region for different number of N beamlets.

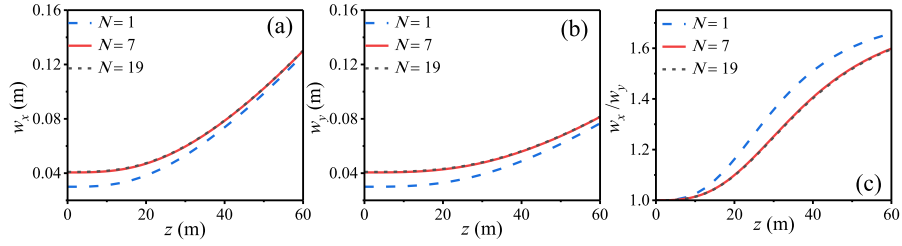

Fig. 10. For different values of number of beamlets N, (a) w_x, (b) w_y, and (c) w_x/w_y versus propagation distance z.

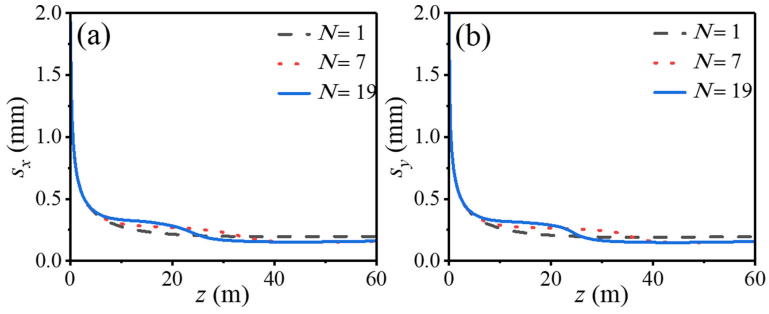

Fig. 11. The effective width of DOC for different numbers of beamlets N versus the propagation distance z in the x and y directions respectively.

see that the beamlets spread faster for the larger value of N. However, the distributions of spectral density are little different for different values of N at $z = 50$ m.

For further study, we show the beam widths w_x and w_y in the x and y directions and the ratio of w_x to w_y versus the propagation distance z for different values of number of beamlets N in Fig. 10, respectively. From Fig. 10, it can be seen that beam width curves of $N = 7$ and 19 coincide perfectly at any propagation distance. Whereas, the value of beam width for a single GSM beam is smaller than that of the GSM beam array, and the single GSM beam spreads more rapidly. The main reason is that the single beam distribution is more concentrated than that of the array beam with a same truncation parameter. Thus, the single beam has a smaller beam width at the source plane. In addition, one can see that the elliptical shape spectral density distribution of array beam is more noticeable than that of a single beam (see Fig. 10(c)).

Fig. 11 shows the effective coherence width for different numbers of beamlets N versus the propagation distance z in the x and y directions respectively. It can be seen that the effective coherence width changing laws are basically the same for different N, i.e., the curves decrease rapidly at initial stage and remain the same value after $z = 40$ m. Hence, it can be concluded that the number of beamlets has almost no effect on the beam width and effective coherence width for a GSM beam array when the exit aperture D and the truncation parameter f are consistent with each other.

4. Conclusion

Based on the anisotropic power spectrum of jet engine turbulence proposed by Sirazetdinov *et al.*, the analytical expression for the CSD function of a GSM beam array propagating through a jet engine turbulence has been derived in this paper. According to the analytical expressions, the beam width and coherence properties of a GSM beam array propagating have been illustrated by numerical simulation. Besides, the influences from the number of beamlets N on the mean-squared beam width and the effective width of DOC have been investigated in detail.

The results show that the profile of spectral density and the DOC of a GSM beam array gradually transfer to an elliptical shape as the propagation distance increases. However, the elliptical degree becomes greater with increasing source coherence length. That is to say, low coherence can weaken the jet engine turbulence. Besides, as the source coherence length decreases, the profile of the DOC appears sidelobes and resembles the spectral density distribution in free space. Furthermore, the beam width remains almost unchanged for different values of source coherence length at the same distance when the source coherence length exceeds a threshold value. It is also found that the values of effective coherence width both in x and y directions nearly remain the same after $z = 40$ m for different values of source coherence length. Comparing with the array beam of different number of beamlets, it can be concluded that the number of beamlets has almost no effect on the beam width and effective coherence width for different GSM beam array, when the exit aperture and the truncation parameter are consistent with each other. However, the single GSM beam spreads more rapidly than GSM beam array. The results obtained in this paper will be very useful for applications in optical imaging, ranging, tracking and communication systems of a GSM beam array propagating in a jet engine exhaust environment.

Acknowledgment

The authors wish to thank the anonymous reviewers for their valuable suggestions.

References

[1] L. C. Andrews and R. L. Phillips, *Laser Beam Propagation Through Random Media*, 2nd ed., WA: SPIE Publications Bellingham, 2005.
[2] J. W. Strohbehn, Laser Beam Propagation in the Atmosphere. New York, NY, USA: Springer-Verlag, 1978.
[3] L. Sjöqvist, "Laser beam propagation in jet engine plume environments: A review," in *Proc. SPIE*, vol. 7115, Oct. 2008, Art. no. 71150C.
[4] J. L. Barrett and P. A. Budni, "Laser beam propagation through strong turbulence," *J. Appl. Phys.*, vol. 71, no. 3, pp. 1124–1127, 1992.
[5] C. B. Hogge and W. L. Visinsky, "Laser beam probing of jet exhaust turbulence," *Appl. Opt*, vol. 10, no. 4, pp. 889–892, 1971.
[6] W. M. Isterling, L. J. Cox, M. Dubovinsky, D. H. Titterton, and T. Porter, "Laser interaction with jet engine exhaust induced turbulence," in *Proc. 4th Australian Conf. Laser Diagnostics Fluid Mechanics Combustion*, Adelaide, Dec. 2005, pp. 65–68.
[7] V. S. Sirazetdinov, "Experimental study and numerical simulation of laser beams propagation through the turbulent aerojet," *Appl. Opt.*, vol. 47, no. 7, pp. 975–985, 2008.
[8] C. L. Ding, O. Korotkova, D. L. Li, D. M. Zhao, and L. Z. Pan, "Propagation of Gaussian Schell-model beams through a jet engine exhaust," *Opt. Exp.*, vol. 28, no. 2, pp. 1037–1050, 2020.
[9] D. H. Titterton, "A review of the development of optical countermeasures," in *Proc. SPIE*, vol. 5615, pp. 1–15, Dec. 2004.
[10] G. D. Goodno *et al.*, "Brightness-scaling potential of actively phase-locked solid-state laser arrays," *IEEE J. Sel. Topics Quantum Electron.*, vol. 13, no. 3, pp. 460–472, May/Jun. 2007.

[11] T. Y. Hou *et al.*, "High-power vortex beam generation enabled by a phased beam array fed at the nonfocal-plane," *Opt. Exp.*, vol. 27, no. 4, pp. 4046–4059, Feb. 2019.
[12] C. X. Yu *et al.*, "Coherent combining of a 4 kW, eight-element fiber amplifier array," *Opt. Lett.*, vol. 36, no. 14, pp. 2686–2688, Jul. 2011.
[13] Y. B. Zhu, D. M. Zhao, and X. Y. Du, "Propagation of stochastic Gaussian-schell model array beams in turbulent atmosphere," *Opt. Exp.*, vol. 16, no. 22, pp. 18437–18442, Oct. 2008.
[14] P. Zhou, Y. X. Ma, X. L. Wang, H. C. Zhao, and Z. J. Liu, "Average spreading of a Gaussian beam array in non-Kolmogorov turbulence," *Opt. Lett.*, vol. 35, no. 7, pp. 1043–1045, Apr. 2010.
[15] P. Yue, J. C. Hu, X. Yi, D. L. Xu, and Y. Y. Liu, "Effect of airy Gaussian vortex beam array on reducing intermode crosstalk induced by atmospheric turbulence," *Opt. Exp.*, vol. 27, no. 26, pp. 37986–37998, Dec. 2019.
[16] R. M. Tao, L. Si, Y. X. Ma, P. Zhou, and Z. J. Liu, "Propagation of coherently combined truncated laser beam arrays with beam distortions in non-Kolmogorov turbulence," *Appl. Opt.*, vol. 51, no. 23, pp. 5609–5618, Aug. 2012.
[17] M. M. Tang and D. M. Zhao, "Regions of spreading of Gaussian array beams propagating through oceanic turbulence," *Appl. Opt.*, vol. 54, no. 11, pp. 3407–3411, Apr. 2015.
[18] X. L. Ma, D. J. Liu, Y. C. Wang, H. M. Yin, H. Y. Zhong, and G. Q. Wang, "Propagation of rectangular multi-Gaussian schell-model array beams through free space and non-kolmogorov turbulence," *Appl. Sci.-Basel*, vol. 10, no. 2, Jan. 2020, Art. no. 450.
[19] L. Lu, X. L. Ji, J. P. Deng, and X. Q. Li, "A further study on the spreading and directionality of Gaussian array beams in non-Kolmogorov turbulence," *Chin. Phys. B*, vol. 23, no. 6, Jun. 2014, Art. no. 064209.
[20] D. J. Liu, H. Y. Zhong, G. Q. Wang, H. M. Yin, and Y. C. Wang, "Propagation of a radial phase-locked partially coherent elegant laguerre-Gaussian beam array in non-Kolmogorov medium," *Appl. Phys. B-Lasers O.*, vol. 125, no. 3, Mar. 2019, Art. no. 52.
[21] X. L. Ji, H. T. Eyyubolu, and Y. Baykal, "Influence of turbulence on the effective radius of curvature of radial Gaussian array beams," *Opt. Exp.*, vol. 18, no. 7, pp. 6922–6928, 2010.
[22] S. Golmohammady, M. Yousefi, A. Mashal, and B. Ghafary, "Scintillation and BER analysis of the partially coherent flat-topped array laser beam in the non-Kolmogorov atmospheric turbulence on slant path," *Laser Phys.*, vol. 29, no. 8, Aug. 2019, Art. no. 086201.
[23] D. J. Liu, H. Y. Zhong, G. Q. Wang, H. M. Yin, and Y. C. Wang, "Radial phased-locked multi-Gaussian Schell-model beam array and its properties in oceanic turbulence," *Opt. Laser Technol.*, vol. 124, Apr. 2020.
[24] D. J. Liu and Y. C. Wang, "Evolution properties of a radial phased-locked partially coherent lorentz-gauss array beam in oceanic turbulence," *Opt. Laser Technol.*, vol. 103, pp. 33–41, Jul. 2018.
[25] K. L. Wang and C. H. Zhao, "Propagation properties of a radial phased-locked partially coherent anomalous hollow beam array in turbulent atmosphere," *Opt. Laser Technol.*, vol. 57, pp. 44–51, Apr. 2014.
[26] L. Yu and Y. Zhang, "Free-space to fiber coupling of electromagnetic Gaussian schell-model beams in turbulent marine atmospheric channel," *IEEE Photon. J.*, vol. 10, no. 6, 2018.
[27] M. Salem, T. Shirai, A. Dogariu, and E. Wolf, "Long-distance propagation of partially coherent beams through atmospheric turbulence," *Opt. Commun.*, vol. 216, no. 4-6, pp. 261–265, 2003.
[28] G. Gbur and E. Wolf, "Spreading of partially coherent beams in random media," *J. Opt. Soc. Am. A*, vol. 19, no. 8, 2002, Art. no. 1592.
[29] Y. J. Cai, Q. Lin, Y. Baykal, and H. T. Eyyuboğlu, "Off-axis Gaussian Schell-model beam and partially coherent laser array beam in a turbulent atmosphere," *Opt. Commun.*, vol. 278, no. 1, pp. 157–167, Oct. 2007.
[30] C. Y. Chen, H. M. Yang, Y. Lou, and S. F. Tong, "Second-order statistics of Gaussian Schell-model pulsed beams propagating through atmospheric turbulence," *Opt. Exp.*, vol. 19, no. 16, pp. 15196–15204, Aug. 2011.
[31] X. L. Ji, E. T. Zhang, and B. D. Lu, "Changes in the spectrum of Gaussian Schell-model beams propagating through turbulent atmosphere," *Opt. Commun.*, vol. 259, no. 1, pp. 1–6, Mar. 2006.
[32] D. J. Liu, G. Q. Wang, and Y. C. Wang, "Average intensity and coherence properties of a partially coherent lorentz-gauss beam propagating through oceanic turbulence," *Opt. Laser Technol.*, vol. 98, pp. 309–317, Jan. 2018.
[33] S. A. Shakir, T. T. Clark, D. S. Cargill, and R. Carreras, "Far-field propagation of partially coherent laser light in random mediums," *Opt. Exp.*, vol. 26, no. 12, pp. 15609–15622, Jun. 2018.
[34] F. Wang, X. L. Liu, Y. S. Yuan, and Y. J. Cai, "Experimental generation of partially coherent beams with different complex degrees of coherence," *Opt. Lett.*, vol. 38, no. 11, pp. 1814–1816, 2013.
[35] G. F. Wu and Y. J. Cai, "Detection of a semirough target in turbulent atmosphere by a partially coherent beam," *Opt. Lett.*, vol. 36, no. 10, pp. 1939–1941, May 2011.
[36] A. L. Yang, E. T. Zhang, X. L. Ji, and B. D. Lü, "Angular spread of partially coherent Hermite-cosh-Gaussian beams propagating through atmospheric turbulence," *Opt. Exp.*, vol. 16, no. 12, pp. 8366–8380, 2008.
[37] Y. S. Yuan, Y. J. Cai, J. Qu, H. T. Eyyuboglu, Y. Bayka, and O. Korotkova, "M-2-factor of coherent and partially coherent dark hollow beams propagating in turbulent atmosphere," *Opt. Exp.*, vol. 17, no. 20, pp. 17344–17356, Sep. 2009.
[38] S. J. Zhu, Y. J. Cai, and O. Korotkova, "Propagation factor of a stochastic electromagnetic Gaussian Schell-model beam," *Opt. Exp.*, vol. 18, no. 12, pp. 12587–12598, Jun. 2010.
[39] M. R. Whiteley and S. Gordeyev, "Conformal phased array aero-optical modeling and compensation," *Opt. Eng*, vol. 52, no. 7, Jul. 2013, Art. no. 071409.
[40] D. Zhi, Y. Z. Chen, R. M. Tao, Y. X. Ma, P. Zhou, and L. Si, "Average spreading and beam quality evolution of Gaussian array beams propagating through oceanic turbulence," *Laser Phys. Lett.*, vol. 12, no. 11, Nov. 2015, Art. no. 116001.
[41] O. Korotkova, *Random Light Beams: Theory and Applications*. Boca Raton: Crc Press, 2013.
[42] F. Wang and O. Korotkova, "Random optical beam propagation in anisotropic turbulence along horizontal links," *Opt. Exp.*, vol. 24, no. 21, pp. 24422–24434, Oct. 2016.
[43] H. Weber, "Propagation of higher-order intensity moments in quadratic-index media," *Opt. Quant. Electron.*, vol. 24, no. 9, pp. S1027–S1049, 1992.